Electron Transition Current Density in Molecules. 2. Ab Initio Calculations for Electronic Transitions in Ethylene and Formaldehyde

Teresa B. Freedman,* Xuling Gao, Mei-Ling Shih, and Laurence A. Nafie*

Department of Chemistry and W. M. Keck Center for Molecular Electronics, Syracuse University, Syracuse, New York, 13244-4100

Received: July 17, 1997; In Final Form: January 5, 1998

We present the first examples of ab initio calculations of electron transition current density (TCD) maps in molecules. Expressions for TCD, derived previously, are implemented at the ab initio level for the $\pi-\pi^*$ transition in ethylene and the $\pi-\pi^*$ and $n-\pi^*$ transitions in formaldehyde, with the CI-singles approximation for the excited states. The vector field calculations of the TCD were carried out utilizing an adaptation of Gaussian 92 and displayed with the AVS software program package. The TCDs can be viewed in various planes to achieve the perspective desired. In the case of the $\pi-\pi^*$ transitions, large vector-field components can be seen along the direction of the allowed electric dipole transition moment. Minor components perpendicular to the principal direction can also be seen, which integrate to zero over the volume of the molecule and do not contribute to the electric dipole transition moment. For formaldehyde, distinct contributions from $\pi-\pi^*$ and $n_y - 3p_x$ configurations are observed. For the $n-\pi^*$ transition in formaldehyde, the magnetic dipole character of this transition is apparent from the circulation of TCD about the C═O bond axis at both the oxygen and the carbon centers. In addition, the electric quadrupole character of this transition is apparent in the *xy*-symmetric pattern of the TCD in a region midway along the C═O bond. We conclude that TCDs of electronic transitions provide new insight into the spatial character and composition of such transitions, which should prove useful in relating the results of quantum mechanical calculations to molecular electronic structure and dynamics.

Introduction

The visualization of the flow of electron density brought about by an electronic transition in a molecule provides new insight into the nature of electronic excitation. Transitions between electronic states in molecules are typically characterized by their symmetry species, the allowed or forbidden character, and the numerical value of the dipole or rotatory strength for a transition effected by various operators or perturbations (electric dipole, magnetic dipole, electric quadrupole, etc.). A sense of the spatial changes in electron density between initial and final states can be obtained from electron density difference maps between the two states, but such maps provide only a static picture, a scalar field indicating electron density decrease or increase, with no specific description of the pathways associated with the motion of the electron density during the transition process. In contrast, electron transition current density (TCD), derived earlier[1] and in the first paper in this series,[2] is a vector field that provides a detailed map of the flow of electron density (current density) for the transition. We present here the first ab initio implementation of the theoretical expressions for TCD and demonstrate how visualization of TCD maps for simple molecules can probe the spatial detail and symmetry properties of electronic transitions. The third paper in this series,[3] an implementation of transition current density expressions for vibrational transitions, illustrates the use of vibrational TCD maps to view electron density flow due to nuclear motion.

Implementation of Theory

As derived in paper 1 in this series,[2] for an electronic transition between stationary states e and e′, we can define a one-particle electron transition probability density (TPD) as

$$\Theta^0_{ee'}(\mathbf{r}) = \int \psi^0_e(\mathbf{r}, \mathbf{r}_2, ..., \mathbf{r}_N)\, \psi^0_{e'}(\mathbf{r}, \mathbf{r}_2, ..., \mathbf{r}_N)\, d\mathbf{r}_2 ... d\mathbf{r}_N \equiv \psi^0_e(\mathbf{r})\, \psi^0_{e'}(\mathbf{r}) \quad (1)$$

where $\psi^0_{e'}(\mathbf{r}, \mathbf{r}_2, ..., \mathbf{r}_N)$ is a pure electronic multielectron wave function with electron 1 unlabeled. The superscript zeros in eq 1 refer to the equilibrium geometry of one of the states, typically the ground electronic state. The wave function product is integrated over all coordinates except those of electron 1 to yield the one-particle electron density function, as indicated by the second equality in eq 1. Subsequent density function expressions below assume implicitly that such integration has been carried out. A more detailed derivation of this density function and those below, starting from time-dependent vibronic wave functions, is given in ref 2.

The TPD represents the time-independent amplitude of the oscillating probability density arising from the coupling of the two stationary states owing to a perturbation. The transition dipole density (TDD), defined as

$$\mathbf{M}^0_{ee'}(\mathbf{r}) \equiv \mathbf{r}\Theta^0_{ee'}(\mathbf{r}) = \psi^0_e(\mathbf{r})\mathbf{r}\psi^0_{e'}(\mathbf{r}) \quad (2)$$

is a vector field that is the position-weighted TPD and also the integrand of the position form of the electric dipole transition moment.[2] The one-particle electron transition current density (TCD), defined as

$$\mathbf{J}^0_{ee'}(\mathbf{r}) = \frac{\hbar}{2m}\int \psi^0_e(\mathbf{r}, \mathbf{r}_2, ..., \mathbf{r}_N)\nabla\psi^0_{e'}(\mathbf{r}, \mathbf{r}_2, ..., \mathbf{r}_N) - \psi^0_{e'}(\mathbf{r}, \mathbf{r}_2, ..., \mathbf{r}_N)\nabla\psi^0_e(\mathbf{r}, \mathbf{r}_2, ..., \mathbf{r}_N)\, d\mathbf{r}_2 ... d\mathbf{r}_N \equiv \frac{\hbar}{2m}[\psi^0_e(\mathbf{r})\nabla\psi^0_{e'}(\mathbf{r}) - \psi^0_{e'}(\mathbf{r})\nabla\psi^0_e(\mathbf{r})] \quad (3)$$

S1089-5639(97)02345-1 CCC: $15.00
Published on Web 04/18/1998

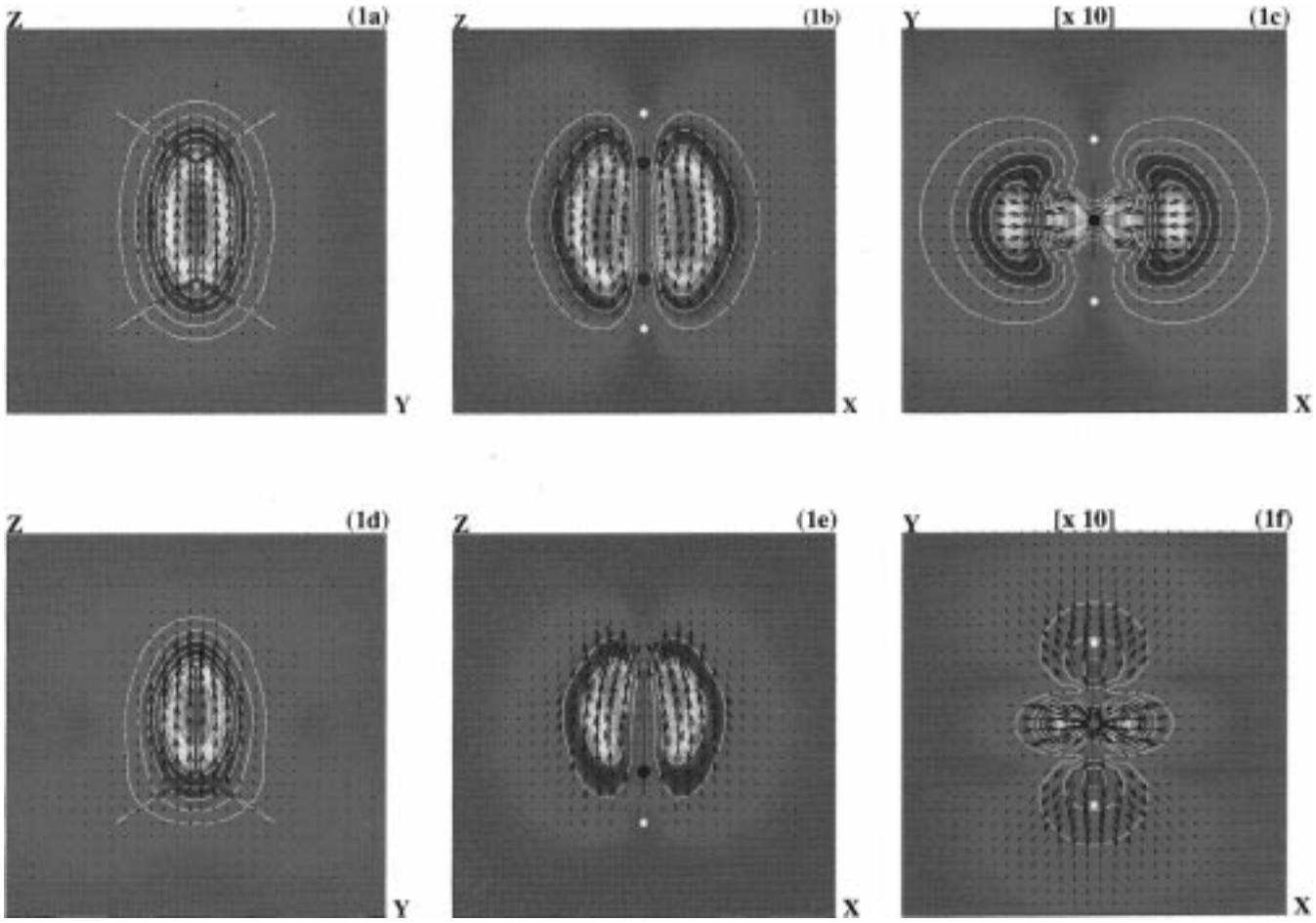

Figure 1. Transition current density plots for the $\pi-\pi^*$ transitions in ethylene (upper diagrams) and formaldehyde (lower diagrams). Color map [red (largest) → blue (smallest)] and contours denote the magnitudes of the TCD vectors, which are projected in a 2D-plane. (a, d) *yz*-projections 0.5 Å above molecular plane; (b, e) *xz*-projections in plane containing double bond and perpendicular to molecular plane; (c) *xy*-projection at the lower carbon atom in ethylene; (f) *xy*-projection at oxygen atom in formaldehyde. Phase of the TCD for the formaldehyde transition has been selected to coincide with the arbitrary phase depicted for the ethylene transition.

is the time-independent amplitude of the current density oscillation between the two coupled stationary states.[2] The TCD is a vector field that is closely related to the integrand of the velocity form of the electric dipole transition moment from state e to e′, namely

$$(\mu_\nu)_{ee'} = -\int \psi_e^0(\mathbf{r}) e\dot{\mathbf{r}} \psi_{e'}^0(\mathbf{r})\, d\mathbf{r} = -\int \psi_e^0(\mathbf{r}) \left(\frac{-ie\hbar}{m}\nabla\right) \psi_{e'}^0(\mathbf{r})\, d\mathbf{r} \tag{4}$$

$$= \frac{ie\hbar}{2m}\int [\psi_e^0(\mathbf{r})\nabla\psi_{e'}^0(\mathbf{r}) - \psi_{e'}^0(\mathbf{r})\nabla\psi_e^0(\mathbf{r})]\, d\mathbf{r}$$

$$= -ie\int \mathbf{J}_{ee'}(\mathbf{r})\, d\mathbf{r} \tag{5}$$

As shown previously,[2] the TCD and TPD satisfy the continuity relationship for the conservation of probability and current density

$$-\nabla\cdot\mathbf{J}_{ee'}^0(\mathbf{r}) = \omega_{e'e}^0 \Theta_{ee'}^0(\mathbf{r}) \tag{6}$$

where $\omega_{e'e}^0 = \omega_{e'}^0 - \omega_e^0$ is the transition frequency given by the frequency difference between the two stationary electronic states.

Plots of TCD were first presented for simple cases involving combinations of atomic s and p orbitals.[1] We have now implemented calculations of TCD using eq 3 through ab initio computation of the TCD vector field and visualization of the TCD maps for the $\pi-\pi^*$ transition in ethylene and $\pi-\pi^*$ and $n-\pi^*$ electronic transitions in formaldehyde. For this initial presentation of such transition current density plots and for comparison to previous examination of these transitions with charge density distribution difference plots,[4,5] we have utilized the configuration interaction with the all single excitations (CIS)[6] method and employed a basis set denoted 6-311(2+,2+)G**, which augments 6-311G with two diffuse sp shells on carbon and one diffuse s shell on hydrogen. This basis set produced the best agreement with experimental vertical transition energies in the earlier work.[4,5] With this method and basis set, the $\pi-\pi^*$ valence state of ethylene (B_{1u} symmetry) is a mixture of three predominant single excitations, whereas the valence $2A_1$ state of formaldehyde is predominantly $\pi-\pi^*$ (three predominant single excitations) with an admixture of some $n_y - 3p_x$ configurations (four predominant single excitations). The vertical $n-\pi^*$ single excitation (A_2) in formaldehyde is a linear combination of three predominant single excitations. Implementation of eq 3 with the CIS method reduces to substitution of the molecular orbital ϕ(occupied) for ψ_e^0 and the appropriate linear combination of molecular orbitals ϕ(virtual) for $\psi_{e'}^0$. The nuclear positions are identical in both states and have been calculated at the MP2/6-31G* level, which gives good agreement with the experimental geometries.

The calculations of the TCD with eq 3 have been carried out by adaptation of the routine (Link 604) in Gaussian 92[7] that calculates orbitals, density, density gradient, and density divergence over a three-dimensional grid of points. Input for this

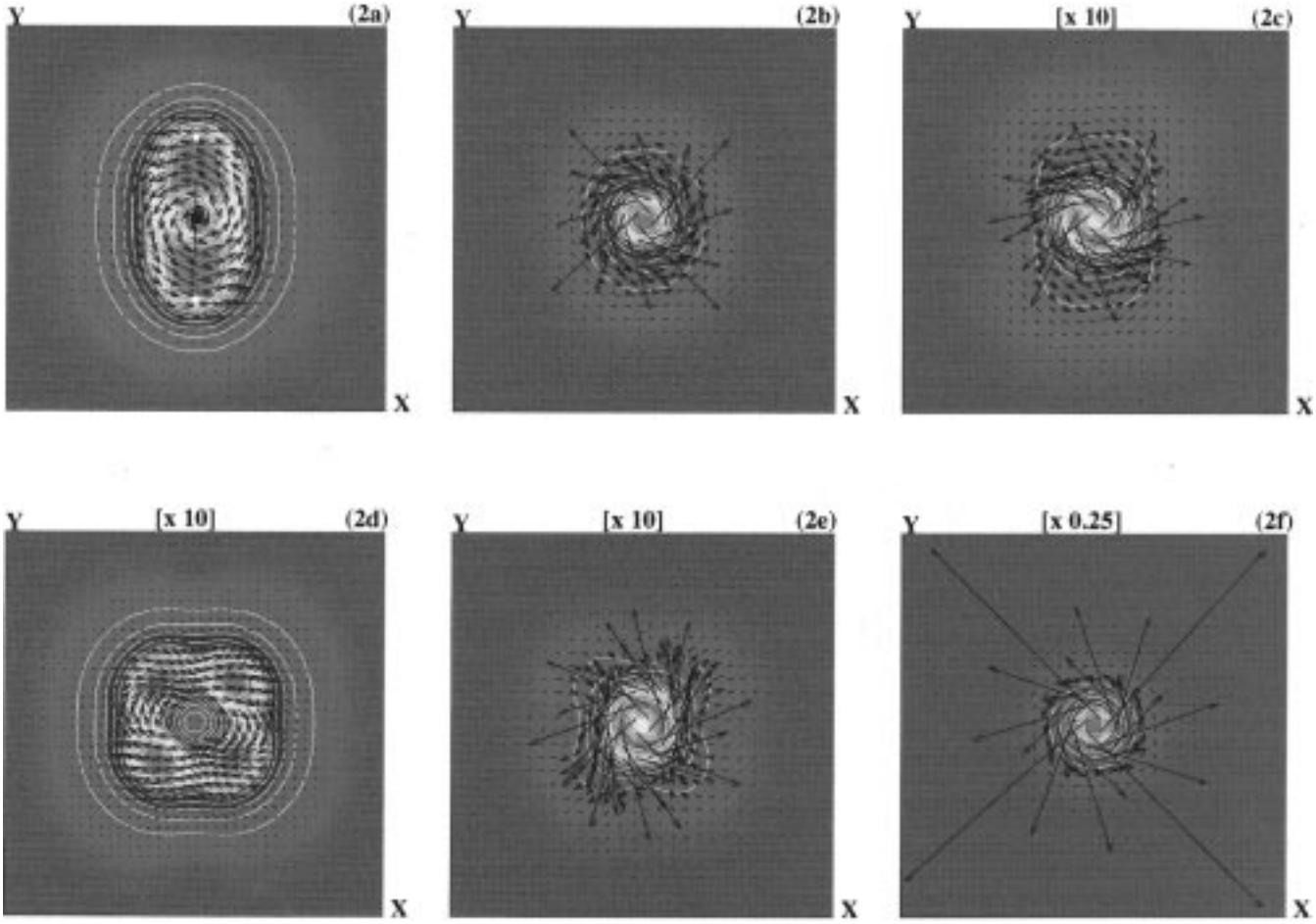

Figure 2. Transition current density plots for the n−π* transition in formaldehyde. (a) *xy*-projection at the hydrogen atoms; (b−f) *xy*-projections viewed along the C═O bond at the carbon atom (b), $^1/_4$ the bond length from the carbon atom (c), at bond midpoint (d), $^5/_{12}$ the bond length from the oxygen atom (e), and at the oxygen atom (f). Grid spacing in (d) has been decreased to reveal detail.

SCHEME 1

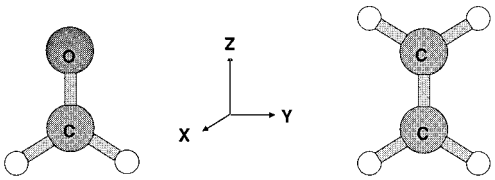

calculation was obtained from the Gaussian 92 or Gaussian 94[8] checkpoint file for a single-point calculation at a previously optimized geometry of each molecule. The resulting three-dimensional TCD vector field has been projected onto selected two-dimensional planes for a practical mode of presentation. The AVS visualization software (Advanced Visual Systems, Inc., Waltham, MA), running on an HP-700 workstation, was employed for display. AVS networks were constructed to plot TCD vectors over the selected grid, superimposed on contoured color maps to further delineate the magnitudes of the projected vectors. These plots have also been superimposed on stick or ball-and-wire representations of the molecular geometry. The AVS Chemistry Viewer (Molecular Simulations, Inc., Burlington, MA) was employed to plot the molecular orbitals and the ball-and-wire or stick models of the molecule from the formatted Gaussian 92/94 checkpoint file for the calculation.

Results

The orientations of ethylene and formaldehyde employed in these calculations are shown in Scheme 1.

Contours of several of the occupied and virtual molecular orbitals involved in the transitions have been previously depicted in the work of Wiberg and co-workers[4,5] and have been reproduced in our study. We note that, in formaldehyde, the nonbonding n_y orbital encompasses both the oxygen and carbon atoms and the π* orbitals have a larger contribution at the carbon. Many of the virtual orbitals for both molecules are quite diffuse, with those contributing to Rydberg states considerably more diffuse than those for valence states. For these TCD calculations on valence transitions we have considered only the region of large overlap with the π or n_y orbital.

Comparison of the $\pi-\pi$* transition current density in ethylene and formaldehyde is shown in Figure 1 for three perpendicular projection planes. The n−π* transition current density in formaldehyde is examined in a series of slices along the C═O bond (Figure 2) and in planes 0.5 Å above and below the molecular plane (Figure 3). Further decomposition of two formaldehyde TCD projections into contributions from single excitations is shown in Figure 4. In Figures 1−4, the relative scales for the sizes of the displayed TCD vectors have been chosen for clarity of presentation of each projection, with relative scales indicated in each figure. In comparing calculated TCD in various planes, we find that the largest *xy*-vector projections in Figure 1c,f are in fact approximately 10 times smaller in magnitude than those in the *xz*- and *xz*-planes. Similarly, in Figure 3, the relative magnitudes of the largest TCD vectors in Figure 2a−f are in the approximate ratios 2:10:1:0.1:1:80. An appreciation of the range of TCD magnitudes in Figure 2a−f

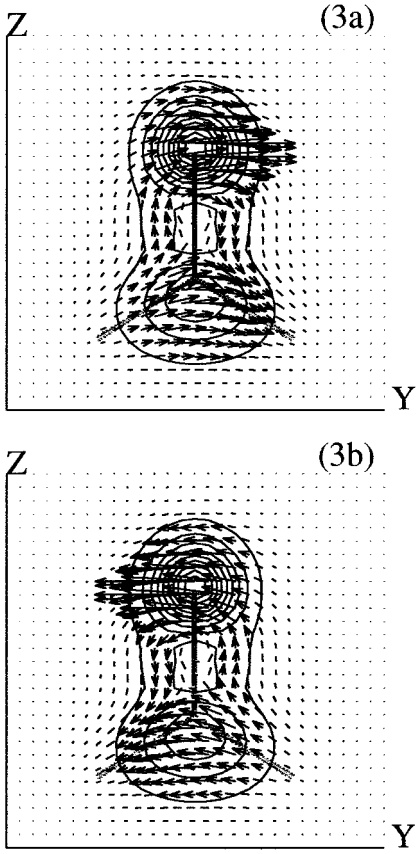

Figure 3. Transition current density plots for the n$-\pi^*$ transition in formaldehyde. (a) *yz*-projection 0.5 Å above molecular plane; (b) *yz*-projection 0.5 Å below molecular plane.

can be obtained from the views above and below the bond plane in Figure 3, where it can be seen that the most intense region is at the oxygen atom and the next most intense region is at the carbon atom.

In Figure 4a−c, the n$-\pi^*$ TCD at the midpoint of the C═O bond from Figure 2d is decomposed into contributions from the three major contributing single excitations. For comparison to ethylene, the *xy*-projection of the $\pi-\pi^*$ TCD at the carbon in formaldehyde is shown in Figure 4d and decomposed into contributions from $\pi-\pi^*$ configurations (Figure 4e) and $n_y - 3p_x$ configurations (Figure 4f).

The overall TCD patterns calculated here are repeated in calculations carried out with the single-transition approximation (a transition between a single occupied and single virtual orbital) with smaller basis sets that do not include extra diffuse orbitals or heavy atom d orbitals (6-31G*, 6-31G, 3-21G, STO-3G basis sets), but the more subtle details of flow patterns and the positions along the C═O bond of the patterns depicted in Figure 2 vary with basis set. In particular, less detail in the TCD patterns is observed in the smaller basis set calculations, and the $n_y - 3p_x$ configuration does not contribute to the $\pi-\pi^*$ transition in formaldehyde.

Discussion

Visualization of transition current density is a new theoretical tool for probing electronic structure. The electron transition current density plots in Figures 1−4 convey a clear spatial representation of the flow of electron density for an electronic transition. We emphasize that this is an oscillating current, only one arbitrary phase of which is shown in the diagrams. Utilization of the momentum operator **p** (or equivalently the velocity operator $\dot{\mathbf{r}}$) in the formulation of TCD (which leads to the vector gradient operator for the electrons) results in a unique, well-defined current vector at each point in space. In contrast, the corresponding vector field representing the transition dipole density (TDD) from eq 2, $\mathbf{r}\theta^0_{ee'}(\mathbf{r})$, which utilizes the position operator **r**, is dependent on the choice of origin, and all vectors point radially away from or toward this origin. Although the integrated form of the TDD (the dipole strength) is origin-independent, there is no unique vector presentation of the TDD itself. Similarly, transition densities derived with the angular momentum operator $\mathbf{r} \times \mathbf{p}$ would yield transition angular current density, which is equivalent to magnetic dipole transition current, and electric quadrupole transition densities could be formulated in a corresponding fashion by utilizing the electric quadrupole operator. Both the magnetic dipole and electric quadrupole transition densities (the integrands of the corresponding transition moments) depend on the choice of molecular origin (as do their integrated forms), and neither would define unique values at each point in space. Thus, the electron transition current density (TCD) is the only form of these transition densities that results in a unique vector field.

The TCD plots for ethylene and formaldehyde presented here reveal clear patterns of electron flow with linear and angular characteristics. For the $\pi-\pi^*$ transitions, the *z*-allowed character of the transition (B_{1u} for ethylene and A_1 for formaldehyde) is apparent from the overall direction of TCD current flow in the $+z$-direction both above and below the molecular plane for the phase of oscillating current shown. Current is zero in the molecular plane, a node for both types of molecular orbital involved in the transition, and the TCD extends outward from the double bond to the greatest extent at the bond midpoint. The maximum TCD magnitude lies closer to the oxygen atom in formaldehyde. The deviations from strictly linear flow are quite apparent in the *xz*-planar projection (Figure 1b,c), with larger angular variation in the formaldehyde transition. In the *xy*-plane (Figure 1c,f), the current vector projections are a factor of 10 smaller than the *z*-components. Distinct differences are observed between the ethylene and formaldehyde transitions in the *xy*-projections. In ethylene, for this phase of TCD, we find that the current in the *xy*-plane flows away from the upper carbon nucleus for one of the contributing single excitations and radially toward the nucleus for a second excitation (Figure 1c), and in the opposite respective directions for the lower carbon (not shown). For formaldehyde, the flow at the oxygen (Figure 1f) is radially toward the nucleus primarily along the *x*-direction, opposite to the flow at the lower carbon in the ethylene transition, for the $\pi-\pi^*$ contribution, but radially away from the nucleus primarily along the *y*-direction for the $n_y - 3p_x$ contribution. At the carbon in formaldehyde (Figure 4d), the overall TCD is generated by a $\pi-\pi^*$ contribution (Figure 4e) quite similar to the overall $\pi-\pi^*$ TCD at the upper carbon in ethylene (Figure 1c), and a $n_y - 3p_x$ contribution (Figure 4f) flowing toward the carbon along the *y*-direction. In all cases, the minor *x*- or *y*-components of the TCD vectors integrate to zero over the plane, as required by symmetry.

The vertical $n_y-\pi^*$ transition in formaldehyde has A_2 symmetry and is a magnetic dipole allowed transition with R_z-character (rotation about the *z*-axis). The *yz*-projection in Figure 3a of the TCD in a plane 0.5 Å above the molecular plane reveals a flow generally in the positive *y*-direction at the carbon and oxygen nuclei, but with circulation in the $\pm z$-direction along the bond midpoint. In the plane 0.5 Å below the molecular plane (Figure 3b), all the projected TCD arrows reverse direction, in contrast to those for the $\pi-\pi^*$ transition, since

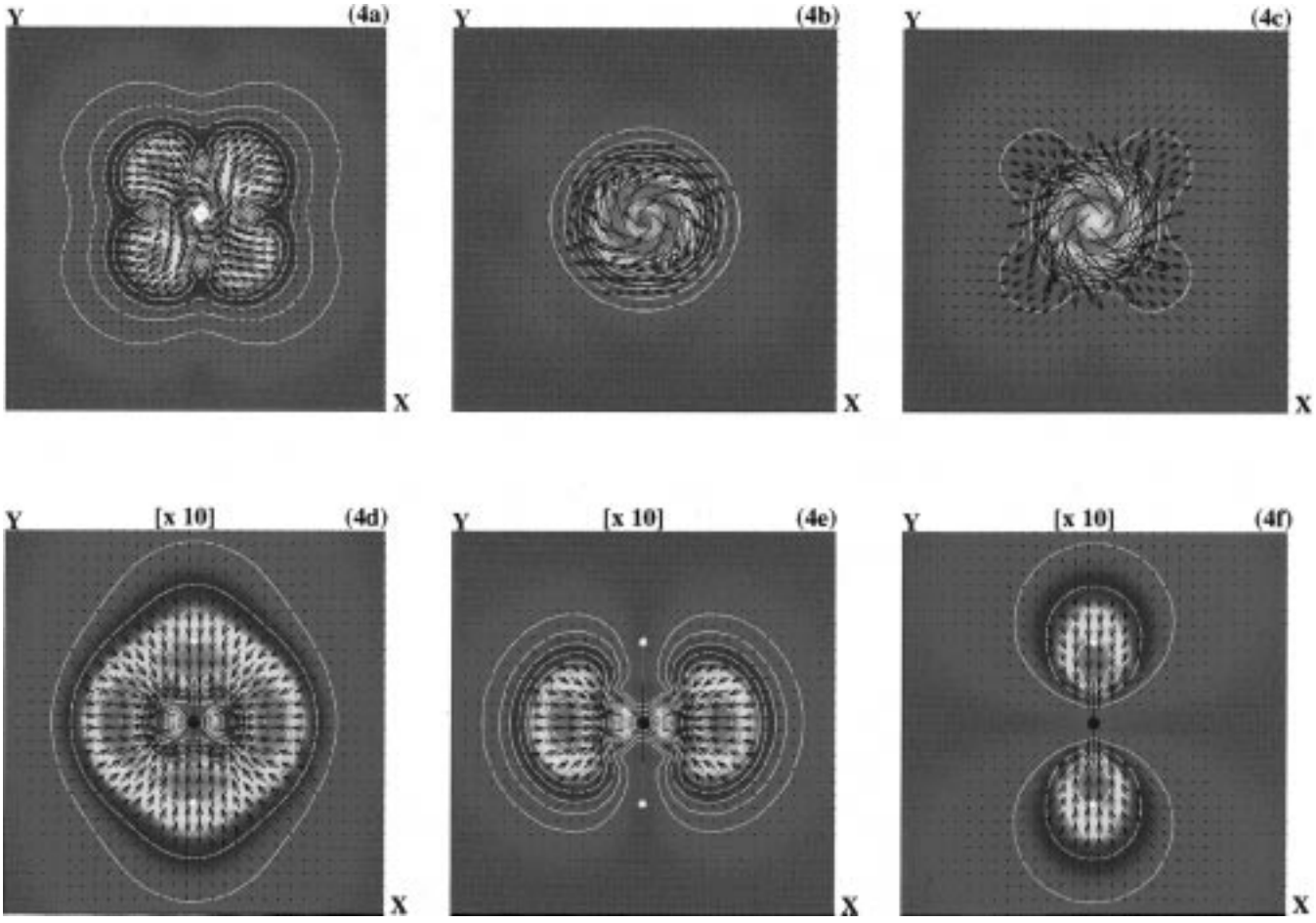

Figure 4. Transition current density plots for formaldehyde. (a−c) Contributions from single excitations to the TCD for the n−π* transition, *xy*-projection at the C═O bond midpoint. Grid spacing in (a) has been decreased to reveal detail. (d−f) *xy*-projection of the transition to the $2A_1$ state at the carbon atom, showing the total TCD (d), the contribution from the $\pi-\pi$* configuration (e), and the contribution from the $n_y - 3p_x$ configuration (f).

the translational character of any charge flow must integrate to zero for an A_2 transition. The TCD vectors for this transition have no components in the plane of the molecule (i.e., vectors at $x = 0$ have only *x*-components). In two-dimensional *xy*-planar projection slices along the double bond (Figure 2), the symmetry of this transition becomes clear. At planes cutting through either the carbon or oxygen nuclei, the current has a distinct angular pattern that the human eye integrates into rotation about the *z*-axis. That is, when one views the pattern in Figure 2b or f, the resulting transition *angular* current density, arising from an $\mathbf{r} \times \mathbf{p}$ angular momentum operator with origin at the atomic center, is inferred. This is precisely the magnetic dipole allowed, R_z, character of the transition. The current vectors at the oxygen atom are an order of magnitude larger than those at the carbon atom, consistent with the view of this type of n−π* transition as involving primarily rotation from the nonbonding to antibonding oxygen orbitals via an angular momentum operator at the oxygen.

As the projection plane is moved along the C═O bond away from either terminal atom, the circular motion becomes more elliptical and then begins to take on quadrupolar character (Figure 2c,e), while the relative magnitudes of the TCD vectors projected in these planes decrease by another order of magnitude compared to those at the carbon atom. At the bond midpoint (Figure 2d), a striking pattern is calculated, which upon closer inspection is found to have *xy*-symmetry, the same symmetry pattern as a d_{xy} orbital. The overall projected vector magnitudes have decreased at this point by a factor of ∼10 from those in Figure 2c,e. At this position, where local angular momentum (leading to magnetic dipole) effects from the atomic centers are minimal, the electric quadrupole allowed character of this transition is revealed. Of course, the division of TCD into magnetic-dipole and electric-quadrupole contributions is heavily dependent on the choice of gauge, and for this purpose we are assuming the natural of choice of the carbonyl bond axis, for planes of TCD perpendicular to it, as a local origin of reference.

Decomposition of the TCD at this midpoint position (Figure 2d) into contributions from single electron transitions, shown in Figure 4a−c, reveals an even more striking quadupolar contribution from one virtual molecular orbital (Figure 4a), a predominantly magnetic-dipolar contribution from a second (Figure 4b), and a combination of magnetic-dipolar and quadrupolar character in the TCD for the third contribution (Figure 4c). We again note that, whereas a **p**-operator property, electron transition current density, is calculated and plotted over a grid of points encompassing the molecule, visual integrations of the overall patterns reveal symmetry properties that are characteristic of all orders of the electromagnetic interaction.

For both types of transition investigated here, the transition current density vectors are largest in the vicinity of the carbons or oxygen and along the double bond. From symmetry, the hydrogen atomic orbitals do not contribute to either the π or π* orbitals, and TCD near the hydrogens is quite small in the $\pi-\pi$* transitions. The hydrogen orbitals do contribute to the n_y orbital in formaldehyde, and, for the $n_y-\pi$* transition, the TCD extends along the CH bonds to the hydrogen nuclei, where

there continues to be angular circulation of electron current around the molecule, with increased current flow emanating from the vicinity of the CH bonds, as shown in Figure 2a.

The previous investigation of these transitions with charge density difference plots[4,5] focused in part on use of these plots to classify the Rydberg and valence nature of the excited states. In particular, the form of the density depletion region of the plots was characteristic of the type of transition, with more complex structure observed for the valence transitions. In this initial presentation of transition current density plots, we have included only the lowest energy valence transitions. The TCD plots clearly provide an additional dimension of insight into the nature of these transitions.

The approach based on TCD presented in this paper can be related, in a more general sense, to previous work with one-electron densities to understand the contributions of local chromophoric groups to electronic transitions.[9] Here, two scalar functions were defined in the context of the random phase approximation (RPA), the charge rearrangement density and the transition density. The former corresponds to the difference in the one-electron probability density and the latter to our definition in eq 1 of the transition probability density (TPD). An advantage of these densities is the ease with which they can be combined with operators, such as the electric-dipole moment operator, to visualize whether a particular transition is allowed with this operator or not. In the present paper we have not developed the analogous methodology.

For the TCD, all orders of electron interaction are present, as we illustrated in the case of the n$-\pi^*$ transition in formaldehyde where both magnetic-dipole and electric-quadrupole activity could be visually identified. Nevertheless, it is straightforward to project out, using group theoretical methods, the allowedness of the TCD for any particular transition by dividing the space of the molecule into the appropriate number and location of sectors and relating the TCDs in each of the sectors by group theoretical operations. For the n$-\pi^*$ transition of a carbonyl group, there would be no surviving TCD for electric dipole transitions and the magnetic-dipole component of the TCD could be projected and displayed (utilizing C_4 symmetry). Similarly, the electric-quadrupole component of the TCD could be also obtained. Remaining TCD, not yet projected, would be ascribed to higher-order multipole interactions and numerical noise. We leave such group theoretical decompositions of TCD to a future publication.

The principal goal of this paper is to present the first detailed examples of the calculation and display of TCD in molecules for electronic transitions. For this purpose, we chose two simple molecules and two different types of transitions, one of which was common to both molecules and for which suitable comparisons could be made. We also used electronic wave functions of reasonable accuracy, one that had been used recently in the literature for the purpose of studying the nature of electronic transitions in these kinds of molecules.[4,5] In this way, the essential features of TCDs could be visualized at a reasonable level of accuracy for the purpose of illustration. We are not seeking to extend the quality of the quantum description of these molecules or to use the most sophisticated wave functions that might be applied. We do note that TCDs are a potentially valuable tool for the comparative study of quantum mechanical descriptions of molecular transitions, at any level of sophistication, in that differences in calculated properties can be visualized directly in terms of the electronic oscillatory motion that occurs during such transitions. Regions displaying the largest differences are those most sensitive in the comparison and may point to regions of the molecule where further mathematical enhancement, such as basis function extension, would lead most effectively to improved descriptions.

Conclusions

We have presented here the first ab initio calculations and plots of transition current density for electronic transitions. It is clear that visualization of electron transition current density provides insight into the character of electronic transitions and the symmetry properties of such transitions that amplifies the pure numerical information obtained from the integrated value of a transition moment or the static view of density difference plots. In fact, we find that visualization of TCD also conveys information on higher orders of electromagnetic interaction (electric quadrupole and magnetic dipole) present in the transitions. We have extended these calculations to longer polyenes such as butadiene, acrolein, and fragments of the retinal side chain, which will be reported separately,[10] and to vibrational transitions.[3] Future applications of calculations of electron transition current density in electronic transitions include consideration of various kinds of chemical reactions, conducting polymers,[11−13] and transitions that involve long-range electron transfer.[14,15]

Acknowledgment. The authors acknowledge support of this work from the New York State Center for Advanced Technology in Computer Applications and Software Engineering (CASE) and the W. M. Keck Center for Molecular Electronics, both at Syracuse University, and the National Institutes of Health (GM-23567).

References and Notes

(1) Nafie, L. A. In Molecular and Biomolecular Electronics; Birge, R. R., Ed.; American Chemical Society: Washington, D. C., 1994; Vol. 240, pp 63−80.

(2) Nafie, L. A. *J. Phys. Chem. A* **1997**, *101*, 7826−7833.

(3) Freedman, T. B.; Shih, M.-L.; Lee, E.; Nafie, L. A. *J. Am. Chem. Soc.* **1997**, *119*, 10620−10626.

(4) Wiberg, K. B.; Hadad, C. M.; Foresman, J. B.; Chupka, W. A. *J. Phys. Chem.* **1992**, *96*, 10756−10768.

(5) Hadad, C. M.; Foresman, J. B.; Wiberg, K. B. *J. Phys. Chem.* **1993**, *97*, 4293−4312.

(6) Forseman, J. B.; Head-Gordon, M.; Pople, J. A. *J. Phys. Chem.* **1992**, *96*, 135−149.

(7) Frisch, M. J.; Trucks, G. W.; Head-Gordon, M.; Gill, P. M. W.; Wong, M. W.; Foresman, J. B.; Johnson, B. G.; Schlegel, H. B.; Robb, M. A.; Repologle, E. S.; Gomperts, R.; Andres, J. L.; Raghavachari, K.; Binkley, J., S.; Gonzalez, C.; Martin, k. L.; Fox, D. J.; Defrees, D. J.; Baker, J.; Stewart, J. J. P.; Pople, J. A. *GAUSSIAN 92, Revision C*; Gaussian, Inc.: Pittsburgh, PA, 1992.

(8) Frisch, M. J.; Trucks, G. W.; Schlegel, H. B.; Gill, P. M. W.; Johnson, B. G.; Robb, M. A.; Cheeseman, J. R.; Keith, T.; Petersson, G. A.; Montgomery, J. A.; Raghavachari, K.; Al-Laham, M. A.; Zakrzewski, V. G.; Ortiz, J. V.; Foresman, J. B.; Peng, C. Y.; Ayala, P. Y.; Chen, W.; Wong, M. W.; Andres, J. L.; Replogle, E. S.; Gomperts, R.; Martin, R. L.; Fox, D. J.; Binkley, J. S.; Defrees, D. J.; Baker, J.; Stewart, J. P.; Head-Gordon, M.; Gonzalez, C.; Pople, J. A. *Gaussian 94*, B.3 ed.; Gaussian, Inc.: Pittsburgh, PA, 1995.

(9) Hansen, A.; Bouman, T. D. *J. Math. Chem.* **1992**, *10*, 221−247.

(10) Freedman, T. B.; Shih, M.-L.; Gao, X.; Nafie, L. A. Unpublished results.

(11) Gussoni, M.; Castiglioni, C.; Zerbi, G. In *Spectroscopy of Advanced Materials*; Clark, R. J. H., Hester, R. E., Eds.; John Wiley and Sons: New York, 1991; Vol. 19, p 251.

(12) Castiglioni, C.; Gussoni, M.; Zoppo, M. D.; Zerbi, G. *Solid State Commun.* **1992**, *82*, 13−17.

(13) Zoppo, M. D.; Castiglioni, C.; Verronelli, M.; Zerbi, G. *Synth. Met.* **1993**, *55*, 3919.

(14) Beratan, D. N.; Onuchic, J. N.; Hopfield, J. J. *J. Chem. Phys.* **1985**, *83*, 5325−5329.

(15) Beratan, D. N.; Onuchic, J. N.; Hopfield, J. J. *J. Chem. Phys.* **1987**, *86*, 4488−4498.